A Revised Hilbert-Huang Transformation to Track Non-Stationary Association of Electroencephalography Signals

Xiaocai Shan, Shoudong Huo, Lichao Yang, Jun Cao, Jiaru Zou, Liangyu Chen, Ptolemaios Georgios Sarrigiannis, and Yifan Zhao, *Senior Member, IEEE*

***Abstract*— The time-varying cross-spectrum method has been used to effectively study transient and dynamic brain functional connectivity between non-stationary electroencephalography (EEG) signals. Wavelet-based cross-spectrum is one of the most widely implemented methods, but it is limited by the spectral leakage caused by the finite length of the basic function that impacts the time and frequency resolutions. This paper proposes a new time-frequency brain functional connectivity analysis framework to track the non-stationary association of two EEG signals based on a Revised Hilbert-Huang Transform (RHHT). The framework can estimate the cross-spectrum of decomposed components of EEG, followed by a surrogate significance test. The results of two simulation examples demonstrate that, within a certain statistical confidence level, the proposed framework outperforms the wavelet-based method in terms of accuracy and time-frequency resolution. A case study on classifying epileptic patients and healthy controls using interictal seizure-free EEG data is also presented. The result suggests that the proposed method has the potential to better differentiate these two groups benefiting from the enhanced measure of dynamic time-frequency association.**

***Index Terms*— EEG, transient connectivity, cross-spectrum, Hilbert Huang transform.**

Manuscript received February 5, 2021; revised March 25, 2021; accepted April 21, 2021. Date of publication April 28, 2021; date of current version May 7, 2021. This work was supported in part by the Liaoning Provincial Department of Education Research Funding Project under Grant QN2019010, in part by the Liaoning Science and Technology Plan Project under Grant 20180550047, in part by the Shenyang Science and Technology Plan Project under Grant 18-013-0-58, in part by the Shengjing Hospital Project under Grant MF45, in part by the National Natural Science Foundation of China under Grant 42042045, and in part by the scholarship provided by the University of Chinese Academy of Sciences (UCAS). *(Corresponding author: Liangyu Chen.)*

Xiaocai Shan, Shoudong Huo, and Jiaru Zou are with the Institute of Geology and Geophysics, Chinese Academy of Sciences, Beijing 100029, China.

Lichao Yang, Jun Cao, and Yifan Zhao are with the School of Aerospace, Transport and Manufacturing, Cranfield University, Cranfield MK43 0AL, U.K.

Liangyu Chen is with the Department of Neurosurgery, Shengjing Hospital of China Medical University, Shenyang 110004, China (e-mail: chenly@sj-hospital.org).

Ptolemaios Georgios Sarrigiannis is with the Royal Devon and Exeter NHS Foundation Trust, Exeter EX2 5DW, U.K.

This article has supplementary downloadable material available at https://doi.org/10.1109/TNSRE.2021.3076311, provided by the authors.

Digital Object Identifier 10.1109/TNSRE.2021.3076311

I. Introduction

ELECTROENCEPHALOGRAPHY (EEG) is a powerful technique that can noninvasively study the electrophysiological brain dynamics with high temporal accuracy. EEG has been instrumental in making discoveries about cognition, brain function, and dysfunction [1]. Cognitive, perceptual, linguistic, emotional, and motor processes are fast and take place from tens and hundreds of milliseconds to a few seconds [2]. Neuronal oscillations are embedded in multiplexed and noisy signals, which have been observed with multiple spatial and temporal scales. The non-stationary, asymmetry and non-linear characteristics of EEG have challenged researchers to develop advanced methods to reveal more hidden information.

Time-frequency-based methods are suitable for analysing various fast, dynamic and spatial-temporal cognitive events. Most of the univariate-based time-frequency analysis involves matching EEG timing data to waveform templates. Wavelet Transform (WT) offers superior time and frequency resolution in comparison to other methods, like the Short-Time Fourier Transform (STFT), and is a commonly used tool for finely identifying hidden information in non-stationary signals. Recent studies have used WT in signal decomposition and adaptive filtering [3], EEG source localization [4], computer-aided seizure detection and epilepsy diagnosis [5], and classification of EEG signals [6]. Because the wavelet transform is based on Fourier analysis, using cone sin waves as templates, it has the inherent shortcoming of Fourier spectrum analysis: it can only detect linear phenomena. For example, it can solve inter-wave frequency modulation, but because the basic wavelet has a certain wavelength, it cannot solve intra-wave frequency modulation [7]. Furthermore, WT is limited by the spectral leakage caused by the finite length of the basic wavelet function, the counterintuitive interpretation of fake high-frequency information when analysing true local low-frequency events, and the non-adaptivity of the once set basis wavelet [7].

It is highly debated if neural oscillations are sinusoidal [8]–[10]. Jones *et al.* [8] demonstrated that peaks at specific frequencies in the spectrum can be created by dominant waveform features in the time domain rather than 'sinusoidal' type oscillations. Mazaheri and Jensen [9] proposed a

physiological explanation for the theory that peaks and troughs of oscillatory activity fluctuate asymmetrically, peaks being more strongly modulated than troughs in response to stimuli. Sinusoid-like activity will be observed, even in noise, when signal processing involves sinusoidal filters. Thus, it is difficult for common WT-based approaches to distinguish between sinusoidal versus non-sinusoidal oscillations [1].

Instead of a sine wave template, some researchers use "physiologically defined" waveforms as an analytical regression template to explicitly incorporate neurophysiological principles into EEG data analysis. Cheveigné [11] automatically synthesised multichannel finite impulse response templates by delaying the original data based on the criterion of reproducibility over stimulus repetitions. Cohen [10] proposed a generalized eigen-decomposed cross-frequency coupling framework based on multi-channel covariance matrix and pointed out that the non-sinusoidal waveform of neural oscillations may provide important insights into biophysical processes. Empirical templates are data-driven and defined from the spatio-temporal filters or the output of computational models. However, the effectiveness of this method depends on the accuracy of the template. Physiologically defined waveform templates need to be targeted to each brain region or cognitive process, and even to each individual. In addition, the data used to estimate physiological waveforms always contain noise, and the dependent biophysical hypothesis models may not be verified [1].

Unlike WT with sinusoidal or physiologically defined wavelets, EMD (Empirical Mode Decomposition) is more intuitive and adaptive without any template assumption of the analysed signal [7], which makes it more suitable for describing non-stationary asymmetric and non-linear characteristics of EEG. EMD analyses the behaviour of non-stationary and nonlinear signals by decomposing them into several intrinsic mode functions (IMFs) that admit well-behaved Hilbert transforms. There are many variants of EMD, such as ensemble EMD (EEMD) [12], bivariate EMD (BEMD) [13], multivariate EMD (MEMD) [14], and complete ensemble EMD with adaptive noise (CEEMDAN) [15]. CEEMDAN can provide an exact reconstruction of the original signal and a better spectral separation of the modes with a lower computational cost, overcoming the "mode mixing" problem of EMD and the lack of ability to reconstruct the original signal of EEMD. Since the decomposition is based on the characteristics of the local time scale, with the Hilbert Transform, the IMFs generate instantaneous frequencies as functions of time that separately estimates dynamic structures of different transient information. The final presentations are several energy-frequency-time distributions, designated as the Hilbert spectrum, and phase-time curves.

Detecting and quantifying the interactions between different EEG channel signals can lead to important insights into the dynamic networks that underpin human brain function [16]. Brain functional connectivity is defined as a measurement to evaluate statistic dependence between separated neuronal regions [17]–[20]. Brain synchronization can provide a mechanism for functionally related but spatially distinct neurons to act synergistically [21], [22]. Abnormalities of brain functional connectivity have been reported for numerous brain disorders [23], [24]. By examining the magnitude of linear or nonlinear correlation in the domain of time, frequency, and time-frequency, studying brain functional connectivity between multiple channels has been increasingly considered as a promising approach [25]. In the time domain, the method of synchronization likelihood (SL) is thought to have the ability to detect both linear and non-linear functional interactions between EEG time series [26]–[28]. Seizure prediction and epileptogenic-focus localisation have been investigated using techniques like correlation coefficient [29] and cross-correlation [30]. The correlation between memory performance and quantified brain functional connectivity from EEG has been used to study Alzheimer's diseases [31]. Babiloni *et al.* [26] suggested that the technique of mutual information (MI) is useful for quantifying information transmitted between EEG rhythms in Alzheimer's diseases; MI can also be estimated in the time-frequency domain. In addition, in the time domain, Babiloni *et al.* [26] and Vicente *et al.* [32] introduced a transfer entropy approach, which presented good performance in detecting unknown non-linear interactions. In the frequency domain, magnitude squared coherence (MSC) is the most widely used technique [33]. Based on phase-locking value (PLV), researchers developed an algorithm to track functional connectivity dynamics [34] and found biomarkers with the purpose of seizure prediction in epilepsy [30] as well as object recognition [35] paradigms in healthy subjects. In the time-frequency domain, Chen *et al.* [36] and Wendling *et al.* [37] used STFT to evaluate the dynamic change of brain connectivity. Furthermore, instead of applying the constant size windows as in the STFT, wavelet coherence (WC) also performs well in quantifying time-varying connectivity [33]. Petrantonakis and Hadjileontiadis [38] developed adaptive methods for EEG signal segmentation in the time-frequency domain to effectively retrieve the emotion-related information. Higher time-frequency resolution means better capturing the dynamic non-stationarity and non-linearity of EEG signals [2], which translates to a more reliable estimation of time-varying brain functional connectivity. Therefore, EMD with corresponding frequency analysis could be a promising analysis tool in the study of functional connectivity.

This paper proposes a new time-frequency brain functional connectivity analysis framework, to track the non-stationary association of two EEG signals, based on a Revised Hilbert-Huang Transform (RHHT). One of the highlights of this framework is a novel method of estimating the cross-spectrum, based on the decomposed components. Compared with other time-frequency methods, such as CWT, the proposed method provides a more accurate dynamic time-frequency feature recognition and can be used to dissect the details of dynamic connectivity between brain regions. The effectiveness of this proposed method is validated through simulated and clinical EEG data.

II. Method

The proposed framework, as illustrated in Fig. 1, introduces a CEEMDAN-based Hilbert Transform, namely RHHT,

to track the non-stationary association of two EEG signals. Firstly, the two signals are decomposed by CEEMDAN to obtain the corresponding IMFs. Secondly, the Hilbert Transform is performed on the IMFs of the two signals to obtain the corresponding time-frequency spectrums respectively. The Cross-Spectrum of the two signals is then estimated and validated through a surrogate significance test. The detail of each step is presented below.

A. CEEMDAN

Empirical Mode Decomposition (EMD) can decompose complicated data into a finite and often small number of 'intrinsic mode functions' that admit well-behaved Hilbert transforms [7]. An intrinsic mode function (IMF) must satisfy two conditions: (1) in the whole data set, the number of extrema and the number of zero crossings must be either equal or differ at most by one; and (2) at any point, the mean value of the envelope defined by the local maxima and the envelope defined by the local minima is zero. EMD separates the signal into fast oscillations and slow oscillations. EMD has the problem of "mode mixing", that is, oscillations with very disparate amplitudes exist in one mode or very similar oscillations exist in different modes. To overcome this, Ensemble EMD (EEMD) [12] performs the EMD over an ensemble of the signal plus Gaussian white noise. By filling the entire time-frequency space to take advantage of the dyadic filter bank behaviour of EMD, the addition of white Gaussian noise solves the mode mixing problem. But it creates a new problem that the reconstructed signal includes residual noise, and different realisations of signal plus noise may produce a different number of modes. Complete Ensemble EMD with Adaptive Noise (CEEMDAN) [15], based on EEMD, only needs less than half of the EEMD screening iterations and can accurately reconstruct the original signal by summing the modes.

Given a signal $x[n]$, $\mathrm{n} = 1, \ldots, \mathrm{N}$, where N is the length of the signal $x[n]$, the defined operator $E_j(\cdot)$ produces the j-th mode of $x[n]$ by EMD. Let $w^i \in [0, 1]$, $i = 1, \ldots, I$ be white noise where I is the realizations times of adding noise. Coefficient ε_i allows selecting the signal to noise ratio (SNR) at each stage. CEEMDAN method can be described by the following algorithm:

1. Decompose I realizations $x[n] + \varepsilon_0 w^i[n]$ by EMD to obtain their first modes and compute the average as the first mode $\widetilde{IMF}_1[n]$:

$$\widetilde{IMF}_1[n] = \frac{1}{I}\sum_{i=1}^{I} IMF_1^i[n] = \overline{IMF}_1[n] \quad (1)$$

2. At the first stage (k = 1) calculate the first residue $r_1[n]$:

$$r_1[n] = x[n] - \widetilde{IMF}_1[n] \quad (2)$$

3. Decompose I realizations $\mathrm{r}_1[\mathrm{n}] + \varepsilon_1 \mathrm{E}_1\left(\mathrm{w}^{\mathrm{i}}[\mathrm{n}]\right)$ by EMD to obtain their first modes and compute the average as the second mode $\widetilde{IMF}_2[n]$:

$$\widetilde{IMF}_2[n] = \frac{1}{I}\sum_{i=1}^{I} E_1\left(r_1[n] + \varepsilon_1 E_1\left(w^i[n]\right)\right) \quad (3)$$

4. For k = 2 calculate the k-th residue:

$$r_k[n] = r_{k-1}[\mathrm{n}] - \widetilde{IMF}_k[n] \quad (4)$$

5. Decompose realizations $r_k[n] + \varepsilon_k E_k\left(w^i[n]\right)$, by EMD to obtain their first modes and compute the average as the $(\mathrm{k}+1)^{\mathrm{th}}$ mode $\widetilde{IMF}_{k+1}[n]$:

$$\widetilde{IMF}_{k+1}[n] = \frac{1}{I}\sum_{i=1}^{I} E_1\left(r_k[n] + \varepsilon_k E_k\left(w^i[n]\right)\right) \quad (5)$$

6. Go to step 4 for the next k and perform steps 4 and 5 until the residue is no longer feasible to be decomposed (the residue does not have at least two extrema).
The final residual $R[n]$:

$$R[n] = x[n] - \sum_{k=1}^{K} \widetilde{IMF}_k[n] \quad (6)$$

with K being the total number of modes. The given signal $x[n]$ can be expressed as:

$$x[n] = \sum_{k=1}^{K} \widetilde{IMF}_k[n] + R[n] \quad (7)$$

Equation (7) makes the proposed decomposition complete and provides an exact reconstruction of the original data. Wu and Huang [12] suggested to use small amplitudes of the added noise for data dominated by high-frequency signals, and vice versa. Following then, this paper uses a few hundred realisations and fixed the same SNR for all the stages.

B. Hilbert Transform

The original signal $x(t)$ and its Hilbert transform $y(t)$ constitute its analytic signal $\mathrm{z}(t)$:

$$y(t) = HT(x(t)) = \frac{1}{\pi} P.V. \int_{-\infty}^{\infty} \frac{x(t)}{t-\tau} d\tau \quad (8)$$

$$z(t) = x(t) + iy(t) = a(t)\, e^{i\theta(t)} \quad (9)$$

where P.V. denotes Cauchy principal value, $a(t)$ and $\theta(t)$ denote the instantaneous amplitude and instantaneous phase, respectively. $a(t)$ is the trace envelope and defined as:

$$a(\mathrm{t}) = \sqrt{\mathrm{x}^2(\mathrm{t}) + \mathrm{y}^2(\mathrm{t})} \quad (10)$$

$\theta(t)$ is defined as:

$$\theta(t) = arctan\left(\frac{y(t)}{x(t)}\right) \quad (11)$$

Instantaneous frequency $f(t)$ is defined as the first derivative of $\theta(t)$. Thus,

$$f(t) = \frac{1}{2\pi}\frac{d\theta(t)}{dt} \quad (12)$$

To prevent ambiguities due to phase unwrapping in Equation (12), $f(t)$ can be calculated instead from:

$$f(t) = \frac{1}{2\pi}\frac{x(t)\,y'(t) - x'(t)\,y(t)}{x^2(t) + y^2(t)} \quad (13)$$

where the prime denotes derivative with respect to time. The time-frequency spectrum of signal $x(t)$ is defined as:

$$RHHT_x(t, f(t)) = a(t)\, e^{i\theta(t)} \quad (14)$$

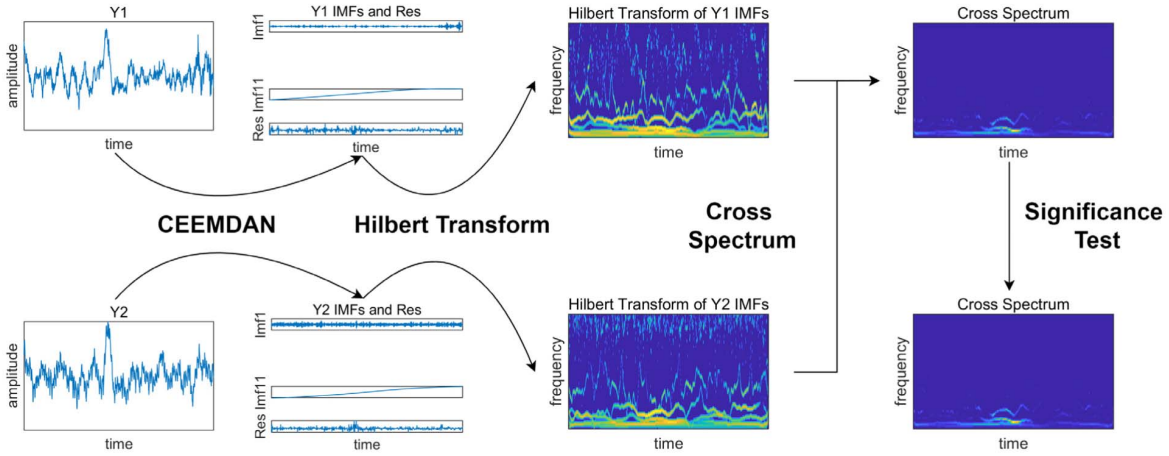

Fig. 1. The flow chart of the proposed framework for tracking non-stationary association based on Revised Hilvert-Huang Transform (RHHT).

The local symmetry property of the IMFs ensures that instantaneous frequencies are always positive, which admits well-behaved Hilbert transforms [7]. The time-frequency spectrum of $\widetilde{IMF}_k(t)$, t = 1, . . . , N, and $k = 1, \ldots, K$, and $R(t)$ are defined as:

$$RHHT_{\widetilde{IMF}_k}(t, f_k(t)) = a_k(t)e^{i\theta_k(t)} \quad (15)$$

$$RHHT_R(t, f_R(t)) = a_R(t)e^{i\theta_R(t)} \quad (16)$$

The time-frequency spectrum of $x(t)$ is:

$$RHHT_x(t, f(t)) = \sum_{k=1}^{K} a_k(t)e^{i\theta_k(t)} + a_R(t)e^{i\theta_R(t)} \quad (17)$$

This procedure produces a multitude of instantaneous frequencies, f including $f_k(t)$ and $f_R(t)$, namely one for each IMF and Residual, allowing for more in-depth signal analysis. At each time point, the instantaneous frequencies are as many as the number of IMFs, and most applications produce up to a dozen IMFs, creating very sparse time-frequency representations. The result is a time-frequency distribution that is uniformly sampled in time but not in frequency, different from the wavelet transform.

C. RHHT Cross-Spectrum

Cross-spectrum can provide information about linear synchronization [39]. The RHHT cross-spectrum of $x_1(t)$ and $x_2(t)$ is defined as follows:

$$SH_{x_1x_2}(t, f) = \int_{t-\delta/2}^{t-\delta/2} RHHT_{x_1}(\tau, f) \cdot RHHT^*_{x_2}(\tau, f)\, d\tau \quad (18)$$

where, $RHHT_{x_1}(\tau, f)$ and $RHHT_{x_2}(\tau, f)$ are the RHHT coefficients $x_1(t)$ and $x_2(t)$ and; * means complex conjugate; δ is the length of the integrating range.

The Continuous Wavelet Transform (CWT) cross-spectrum of $x_1(t)$ and $x_2(t)$ is defined as follows:

$$SW_{x_1x_2}(t, f) = \int_{t-\delta/2}^{t-\delta/2} CWT_{x_1}(\tau, f) \cdot CWT^*_{x_2}(\tau, f)\, d\tau \quad (19)$$

where, $CWT_{x_1}(\tau, f)$ and $CWT_{x_2}(\tau, f)$ is the CWT coefficients $x_1(t)$ and $x_2(t)$; * means complex conjugate; δ is the length of the integrating range.

For CWT cross-spectrum, the length of wavelet transform integral window δ is defined as $\delta = n_{cy}/f$, where n_{cy} is the number of integral cycles in the wavelet window, independent from frequency f, and the length of each cycle is $1/f$. When n_{cy} is fixed, there is an inverse relationship between δ and f. Low frequencies need a greater and a longer data set to average over, as the time resolution is low, and the frequency resolution is relatively high. High frequencies need a small value of δ, as the data need to be superimposed are shorter on average, with time resolution being relatively high and frequency resolution being relatively low. In practical applications, if the data length is short, δ should be a small value, and long data need a bigger value of δ than short data [40]. For RHHT cross-spectrum, the selection of δ is entirely empirical, independent of frequency. In this paper, the length of the integral window of RHHT coherence was set to 4.

Given two signals $x_1(t)$ and $x_2(t)$, For all IMFs of $x_1(t)$ and $x_2(t)$, the RHHT cross-spectrums between $\widetilde{IMF}_{x_{1k}}(t)$ and $\widetilde{IMF}_{x_{2k}}(t)$ can be calculated and analysed separately.

D. Significance Test

A significance test is introduced to assure the data analysis does not reflect our prejudice about the underlying system and that represents a fair account of the structures presented in the data [41]. Consequently, for the data-driven time-frequency analysis by RHHT, the application of this method has to be justified by establishing the statistical significance of the connectivity estimated by cross-spectrum. The method of surrogate data has been a popular tool to address this problem. We first specify the "no connectivity" as our null hypothesis, then generate surrogate data sets that are consistent with this null hypothesis by Amplitude Adjusted Fourier Transform (AAFT) algorithm [42], and finally compute a discriminating statistic for the original and each of the surrogate data sets. If the cross-spectrum value computed for the original data is significantly different than the ensemble of values computed for the surrogate data, then the null hypothesis is rejected

at a given significance level and significant connectivity is detected.

Denote the original time series by $x[n]$, with n = 1, . . . , N. The AAFT algorithm can be summarised below:

1. The first step is to make a Gaussian time series $s[n]$, where each element is generated independently from a Gaussian pseudorandom number generator.
2. Re-order the time sequence of the Gaussian time series so that the ranks of both time series agree, that is, if $x[n]$ is the m^{th} smallest of x, then $s[n]$ will be the m^{th} smallest of s. The re-ordered $s\,[n]$ is a time series that "follows" the original time series $x[n]$ and has a Gaussian amplitude distribution.
3. Using the windowed or unwindowed Fourier Transform algorithm, a surrogate, call it $s'[n]$, of the Gaussian time series can be created. If the original time series $x[n]$ is time re-ordered so that it follows $s'\,[n]$ in the sense that the ranks agree, then the time-re-ordered time series provides a surrogate of the original time series which matches its amplitude distribution. Further, the "underlying" time series ($s[n]$ and $s'[n]$) are Gaussian and have the same Fourier power spectrum.

This procedure was repeated 100 times and then the 95% quantile (z-score = 1.96) was determined as the threshold for each time and frequency point in the time-frequency spectrum.

III. Simulations

This section aims at demonstrating the performance of the proposed method against the wavelet-based method using simulation examples. Each of the two simulated EEG signals has two non-linear signal components, namely the linear frequency increase Chirp signal and the frequency-modulated Cos signal. The sampling frequency is 500Hz, with a length of 1000 (equal to 2s).

The frequency of the first Chirp signal u_1 increases from 30Hz to 40Hz, and the second one u_2 increases from 30Hz to 46Hz, being defined as:

$$u_1 = \cos\left(2\pi\ (f_s + c_1 t) * t\right) \tag{20}$$

$$u_2 = \cos\left(2\pi\ (f_s + c_2 t) * t\right) \tag{21}$$

where f_s is the starting frequency, $f_s = 30Hz$; c_1 and c_2 are chirpiness, $c_1 = 5Hz/s$ and $c_2 = 8Hz/s$. The instantaneous frequency of u_1 and u_2 are:

$$f_{u_1}(t) = \frac{1}{2\pi}\frac{d\theta_{11}}{dt} = f_s + c_1 t \tag{22}$$

$$f_{u_2}(t) = \frac{1}{2\pi}\frac{d\theta_{12}}{dt} = f_s + c_2 t \tag{23}$$

where $\theta_{11} = 2\pi\ (f_s + c_1 t) * t$ and $\theta_{12} = 2\pi\ (f_s + c_2 t) * t$.

The two intrawave frequency-modulated Cos signals v_1 and v_2, showing different harmonic distortion, are defined as:

$$v_1 = \cos\left(2\pi f_a t + 0.5\ sin\ (2\pi f_b t)\right) \tag{24}$$

$$v_2 = \cos\left(2\pi f_a t + 0.5\ sin\ (2\pi f_c t)\right) \tag{25}$$

where f_a is the intrinsic frequency, being $6Hz$; f_b and f_c are the intrawave modulation frequencies, being $6Hz$ and $8Hz$, respectively. The main frequency of v_1 or v_2 exhibits intrawave frequency modulation of nonlinear systems: the further from this equilibrium point, the stronger the nonlinearity [7]. The instantaneous frequency of v_1 and v_2 are:

$$f_{v_1}(t) = \frac{1}{2\pi}\frac{d\theta_{21}}{dt} = f_a + 0.5 f_b \cos(2\pi f_b t) \tag{26}$$

$$f_{v_2}(t) = \frac{1}{2\pi}\frac{d\theta_{22}}{dt} = f_a + 0.5 f_c \cos(2\pi f_c t) \tag{27}$$

where $\theta_{21} = 2\pi f_a t + 0.5 * \sin(2\pi f_b t)$ and $\theta_{22} = 2\pi f_a t + 0.5 * \sin(2\pi f_c t)$.

The two simulated EEG channel signals Y_1 and Y_2 are defined as:

$$Y_1 = 0.8 * u_1 + 0.2 * v_1 + n_1 \tag{28}$$

$$Y_2 = 0.8 * u_2 + 0.2 * v_2 + n_2 \tag{29}$$

White Gaussian noise n_1 and n_2 were added to make the SNR of the observed Y_1 and Y_2 being 40dB. We used the function '*awgn*' in Matlab to add white Gaussian noise to the signals. This function assumes that the power of the input signal is 0 dBW and noisePower is calculated by $\frac{1}{10^{(SNR/10)}}$ dBW. The noise is produced by 'sqrt(noisePower)* randn(size(signal))' in Matlab.

CWT is obtained using the analytic Morlet wavelet. Morlet is one of the most popular wavelet functions for biomedical signals due to its suitability and simplicity [43]. It has several advantages for the time-frequency analysis [44]. Firstly, Morlet convolution keeps the temporal resolution the same as the original signal. Secondly, the Morlet wavelet has a Gaussian distribution in both the time and frequency domain [45], non-sharp edges of which can minimise ripple effects that may be misinterpreted as oscillations. Thirdly, compared to other wavelets, Morlet convolution is more computationally efficient by involving the fast Fourier transform.

Two fine-tuned examples are presented to illustrate that RHHT has the following advantages over CWT: characterizing non-linear interwave with high time-frequency resolution, and capturing sudden changes in frequency and amplitude, which make the RHHT cross-spectrum superior in analyzing the linear connectivity of two-channel signals. The IMF_s from CEEMDAN are compared with the $Band_s$ form Wavelet Convolutional Filter. In order to maintain the consistency of the Wavelet Convolutional Filter, we obtain the corresponding $Band_s$ components by setting the centre frequency and bandwidth parameters as the dominant frequency and bandwidth of the first and second IMF. The RHHT cross-spectrums of Y_1, Y_2 and their corresponding IMF_s are compared with CWT cross-spectrums of Y_1, Y_2 and their corresponding $Band_s$.

A. Example 1

In order to evaluate the performance of the proposed method in capturing similar and dissimilar oscillations within two signals, based on Eq. (24) and Eq. (25), the first half of the v_2 component is adjusted to be the same as the first half of the v_1 component. Fig. 2(a) shows the theoretical instantaneous frequency of Y_1, Y_2 and their components u_1, u_2 and v_1, v_2 respectively. It can be observed from the second row of Fig. 2(a) that u_1 and u_2 have a relatively similar instantaneous

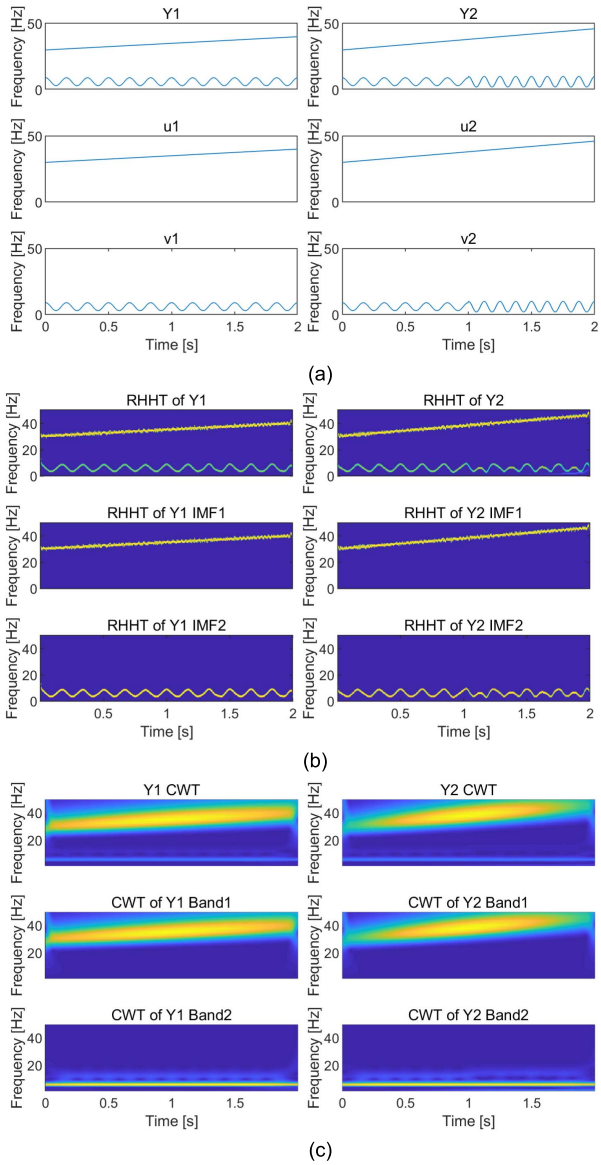

Fig. 2. Example 1 (a) Instantaneous frequency of Y1, Y2 and their components; b) RHHT of Y1, Y2 and associated IMFs; (c) CWT of Y1, Y2 and associated bands.

frequency in the beginning stage and the difference between them increases with time. The instantaneous frequencies of v_1 and v_2 are same in the first half, and the second half is quite different.

Fig. 2(b) and Fig. 2(c) illustrate the time-frequency results of RHHT and CWT. The first row shows the time-frequency maps of Y_1 and Y_2; the second and third rows show the time-frequency maps of Y_1's and Y_2's first and second IMF or band. The estimated instantaneous frequency energy of RHHT in Fig. 2(b) is accurately localised in both frequency and time domains. RHHT spectrums of Y_1 and Y_2 contain two prominent components: the high-frequency component fluctuating increasingly from 30Hz to 40 or 46Hz, and the strongly intrawave frequency-modulated oscillations with intrinsic frequency 6Hz, in agreement with the theoretical instantaneous frequency shown in Fig. 2(a). The observed high time-frequency resolution leads to better characterization of oscillations pattern of Y_1, Y_2 and their components u_1, u_2 and v_1, v_2. For the CWT results shown in Fig. 2(c), neither the energy density nor the frequency is well localized. Corresponding to u_1 and u_2, due to the low resolution of CWT in the high-frequency part, the results of two signals' $Band_1$ spread energy over a much wider frequency range but fail to detect any truly detailed frequency variations. CWT spectrums of two signals' $Band_2$ show a rich distribution of harmonics but no details of the intrawave frequency modulations. The second half period of the two signals' $Band_2$ seems almost the same, which is different from the true theoretical state. This indicates the effective property of the RHHT spectrum in capturing the distortion harmonic components to represent the dynamic signal with modulated frequency.

The RHHT cross-spectrums of Y_1, Y_2 and their corresponding IMFs are shown in Fig. 3(a), where it can be observed from the second column that energy density is well localized within 95% statistical significance. The RHHT cross-spectrum of IMF_1 of Y_1, Y_2 in the second row shows similar time-frequency connectivity in the beginning stage and this connectivity disappears in the second half period, which matches the ground truth shown in Fig. 2(a). The IMF_2 of Y_1, Y_2 in the third row of Fig. 3(a) further confirms this conclusion by successfully picking up the high and consistent association of v_1 and v_2 in the first half period and a less consistent association in the second half. The results of CWT cross-spectrum shown in Fig. 3(b), particularly the ones after the significant test, cannot fully capture the dynamic time-frequency association of the two signals. For example, the limited significant association is detected in $Band_2$ in the first half which should be high and consistent. A significant association is detected in $Band_1$ in the second half period, which is not true.

B. Example 2

In order to simulate the transient property of the non-stationary signal, based on Eq. (24) and Eq. (25), the Chirp and Cos components of the two synthetic EEG signals are adjusted by suddenly changing the frequency and amplitude. The second quarter and the fourth quarter of u_1 are swapped, as is u_2. The amplitude of the first and last quarter of v_1 component is set to zero, while the middle half of v_2 component is set to zero. Fig. 4(a) shows the theoretical instantaneous frequency of Y_1, Y_2 with their components u_1, u_2, and v_1, v_2.

Fig. 4(b) and 4(c) illustrate the time-frequency results of RHHT and CWT. The first row shows the time-frequency maps of Y_1 and Y_2; the second and third rows show the time-frequency maps of the IMFs or Bands of Y_1 and Y_2. It can be observed that the instantaneous frequency results of RHHT are more consistent with Fig. 4(a) than the CWT results. In Fig. 4(b), the time-frequency spectrum of IMF_1 strictly reveals sudden changes of frequency at 0.5s, 1s and 1.5s, and the time-frequency spectrum of IMF_2 undergoes intrawave frequency modulation and captures the sudden changes in amplitude energy at 0.5s, and 1.5s. In Fig. 4(c), the time-frequency results of CWT reveal the transient property of the signal but are encumbered by harmonic components and the edge effects. There is energy dispersion at the sudden changes in frequency and amplitude of the

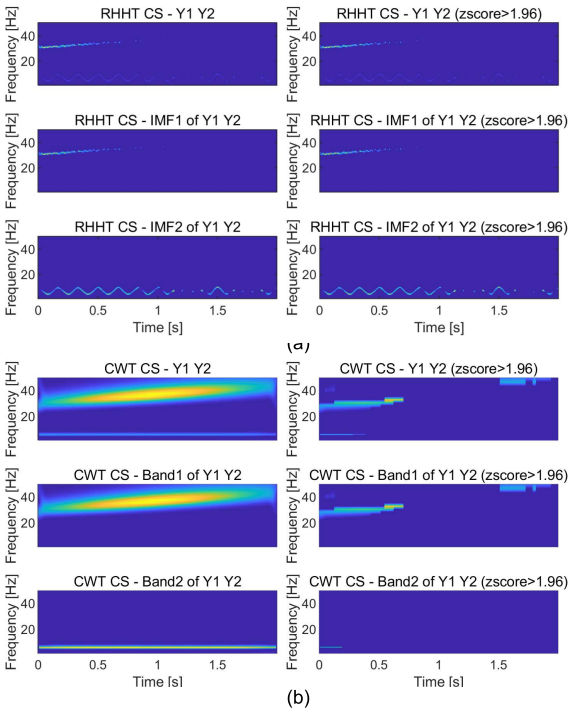

Fig. 3. Example 1 (a) RHHT cross-spectrum (CS) of Y1, Y2, and IMFs before and after significant test; (b) CWT cross-spectrum of Y1, Y2, and associated bands before and after significant test.

two components. This indicates that RHHT spectrum can better capture non-stationarity and reveals more details of the system with a higher resolution.

In the second row of Fig. 5(a), the RHHT cross-spectrum of Y_1 and Y_2's IMF_1 shows similar time-frequency connectivity in the beginning and ending stage, which does not exist in the middle half period, in agreement with the ground truth shown in Fig. 4(a). In the third row of Fig. 5(a), the RHHT cross-spectrum of Y_1 and Y_2's IMF_2 shows low energy of discontinuous connectivity at time 0.5s and 1.5s. However, in Fig. 5(b), CWT cross-spectrum of Y_1 and Y_2's $Band_1$ shows that the connectivity energy exists at some high-frequency areas with statistical significance, which may be caused by the low-frequency resolution. CWT cross-spectrum of Y_1 and Y_2's $Band_2$ show divergent connectivity energy at time 0.5s and 1.5s within a certain time range.

To investigate the effect of and sensitivity to noise, we tested the results of the two synthetic examples with lower SNRs being as 30dB and 20dB, shown in Fig. S2-7 in the Supplementary Material. For the data with the SNR being 30dB, a similar conclusion as that of 40dB can be drawn. For the data with the SNR being 20dB, compared with CWT, RHHT seems to be more sensitive to noise. However, this kind of problem can be addressed by applying a Gaussian filter before the analysis, as shown in Fig. S6 and S7. The superior performance of RHHT is observed again after the Gaussian filter processing.

IV. Application to EEG Data

This section introduces a clinical application of the proposed technique to assist the diagnosis of generalized epilepsy. In this work we retrospectively selected video EEGs (vEEGs)

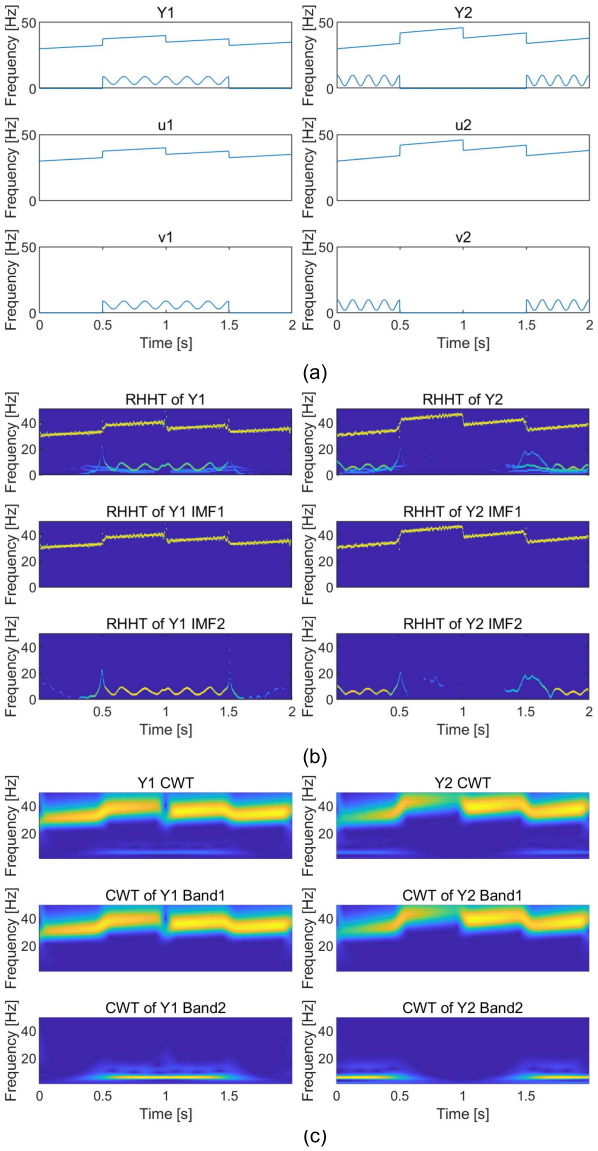

Fig. 4. Example 2 (a) Instantaneous frequency of Y1, Y2 and their components; (b) RHHT of Y1, Y2 and associated IMFs; (c) CWT of Y1, Y2 and associated bands.

with occasional generalised interictal epileptiform discharges (IEDs), providing electrophysiological evidence for the diagnosis of epilepsy. All selected epilepsy patients were isolated from the Royal Hallamshire Hospital (Sheffield, UK) Department of Neurophysiology database with the following inclusion criteria: standard interictal EEG available containing at least one well defined generalised IED; age between late teens to 61 years (based on a cohort of healthy control (HC) available from previous work to ensure no significant age differences between groups occurred); previous history of at least one witnessed generalised tonic-clonic seizure without any other known type of seizures. The following exclusion criteria were also applied: learning difficulties; sleep deprivation the night before the EEG was recorded; the known history of drug addiction; refractory epilepsy; any other known neurological disorder other than epilepsy.

The investigated EEG data comes from two groups: epileptic participants and HC. The data of 10 HC (6 females and

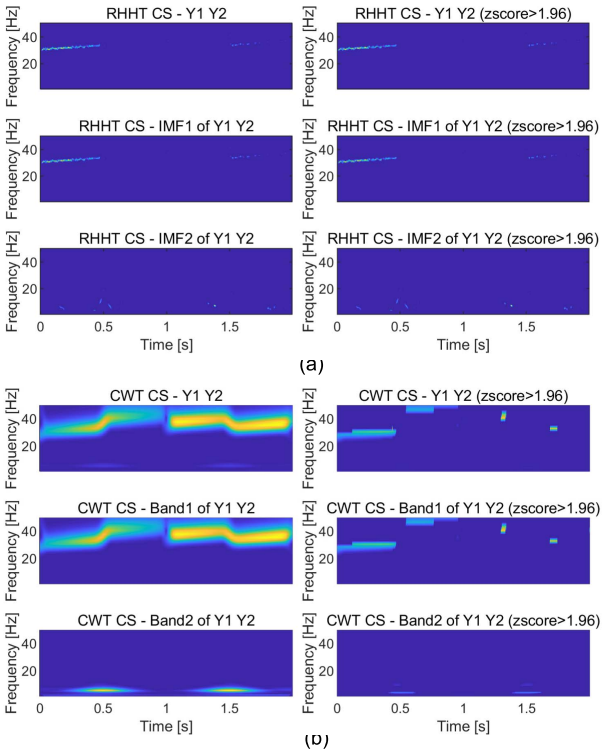

Fig. 5. Example 2 (a) RHHT cross-spectrum (CS) of Y1, Y2 and IMFs before and after significant test; (b) CWT cross-spectrum of Y1, Y2, and bands before and after significant test.

4 males, mean age 37 ± 15y) and 14 epilepsy participants (9 females and 5 males, mean age 33 ± 12y) were collected, details of which can be seen in Table S1 in the Supplementary Material. The epilepsy participants were patients diagnosed with generalized epilepsy and otherwise neurologically normal, without other underlying medical conditions. It should be noted that epilepsy participants were consecutively selected for the best possible match of age to the HC cohort. Additionally, the data for each participant was divided into two states: eyes open (EO) and eyes close (EC). For each subject of each eye state, the epoch lasts 10 seconds. Ethics approval for use of the patients' EEGs for the development of new quantitative EEG methods was obtained both from the University of Sheffield and the NHS ethics committees (SMBRER207 and 11/YH/0414). This All HC subjects provided informed consent as part of a project approved by the Yorkshire and the Humber (Leeds West) Research Ethics Committee (reference number 14/YH/1070). A resting-state standard EEG recording was used. Interictal (i.e. seizure-free) EEG data was selected for this paradigm.

Data was acquired with a Natus Headbox (Optima Medical, Ltd.) at a sampling rate of 500 Hz (analogue bandwidth 0.1–200 Hz) with the international 10–20 system of electrode placement positions. The EEG data was recorded from the standard 21 electrodes.

The EEG epochs were collected with Spike2 (version 9) software where data filtering and labeling were also undertaken. The filtering method was performed using the following equation $y(t) = x(t) - 1/2c \sum_{i=t-c}^{t+c} x(i)'$, where x is the input EEG signal, y is the output signal, t is a discrete-time point and c is a time constant value. The value of c is set at 0.2s. The filtering using a time constant results in a high pass filtering of the signal where the cut-off frequency is $1/2\pi c$, which is equal to 0.79Hz. All data were selected by a specialised physician to ensure no interictal EEG abnormalities were included. Additionally, care was taken to select relatively artefact-free epochs.

A bipolar montage approach was implemented to avoid volume conduction effects caused by the common reference electrode. The following bipolar channels were available: Fp2-F8, Fp1-F7, F8-F4, F7-F3, F4-C4, F3-C3, F4-FZ, FZ-CZ, F3-FZ, T4-C4, T3-C3, C4-CZ, C3-CZ, CZ-PZ, C4-P4, C3-P3, T4-T6, T3-T5, P4-PZ, P3-PZ, T6-O2, T5-O1, P4-O2, P3-O1, O2-O1.

A. RHHT Cross Spectrum

We used C3-P3 as Y_1 and T3-T5 as Y_2 from one epilepsy patient as an example to compare the performance of RHHT and CWT in tracking the non-stationary association of EEG signals. It has been proven in previous research that the connectivity between this pair can provide an insight to differentiate epilepsy group and healthy control group [46]. In the first two rows of Fig. 6(a), the RHHT spectrums of Y_1 and Y_2 show irregularly distributed energy in the high-frequency part above 20Hz, strongly unevenness of the intrawave frequency variation around 5-20Hz frequency band, and low-frequency oscillations below 5Hz with considerable energy. In the third row, RHHT cross-spectrum between Y_1 and Y_2 shows strong oscillations with sharp frequency and time localization. In the last row, RHHT cross-spectrum within a 95% confidence interval shows the connectivity energy of some intrawave frequency oscillations. In the first two rows of Fig. 6(b), the CWT spectrums of Y_1 and Y_2 show smoothed distributed energy in the high-frequency part, some transient energy clusters around intermediate frequency, and almost uniform low-frequency response. In the third row, CWT cross-spectrum between Y_1 and Y_2 is smoother in both time and frequency with spurious harmonics. In the last row, CWT cross-spectrum within a 95% confidence interval shows low connectivity energy in the high-frequency part and strong energy of some connectivity clusters. Comparing the third and last row, some spurious connectivity energy exists in the CWT cross-spectrum without the significant test but disappears in the result with the significant test.

Comparing Fig. 6(a) and 6(b), it is suggested that both cross-spectrums based on RHHT and CWT show similar locations of energy associations in time and frequency axes, but RHHT gives a sharper and more refined definition of the energy than CWT. The intrawave frequency modulations by the RHHT spectrum not only present a clear physical picture of the motion but also eradicate the need for eliminating the spurious harmonics to represent nonlinear and non-stationary signals. All the interesting details pertinent to the similar frequency modulations between the two EEG channels of this paradigm can be seen clearly in the RHHT cross-spectrum, whereas the CWT cross-spectrum only gives a profuse display of harmonics with limited detail.

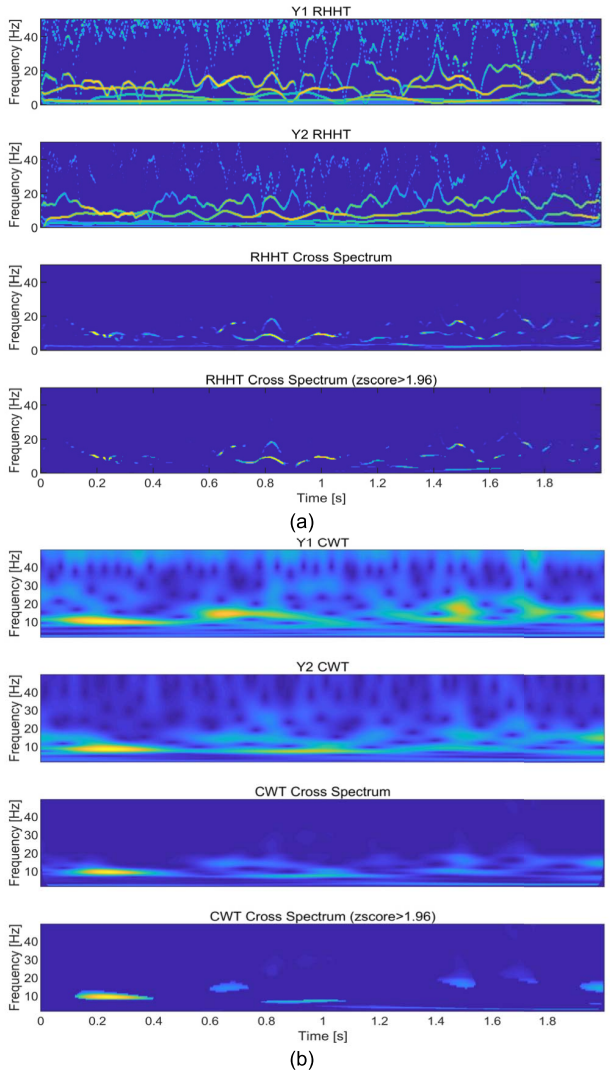

Fig. 6. (a) RHHT of Y1 and Y2 and the cross-spectrum significance result with 95% confidence interval (b) CWT of Y1 and Y2 and the cross-spectrum significance result with 95% confidence interval.

B. Statistical Inference for Potential Classification Benchmark

The Mann-Whitney U test [47], also known as the Wilcoxon rank-sum test, is a nonparametric test for differences between two groups on a single, ordinal variable with no specific distribution. By contrast, the independent-samples t-test, also a test of two groups, requires the single variable to be measured at the interval or ratio level, rather than the ordinal level, and to be normally distributed. When data do not meet the parametric assumptions of a normal distribution, the Mann-Whitney U test tends to be more appropriate [48]. Our data sample size is small and it fails the normal distribution test. Therefore, the Mann-Whitney U test is used in this example to accept or reject the null hypothesis that the epileptic patients and HC samples are samples from continuous distributions with equal medians. If rejected at a critical probability level, typically $p < 0.05$, it infers that the two samples do not come from the same population. The attained p-values can give an idea of the significance level of the results [49].

Considering the estimated measures of cross-spectrum between two signals, with 23 bipolar channels used in this study, there are 253 possible combinations (C_2^{23}) when any 2 bipolar derivations are paired together. These were organised in a pairwise manner by taking the first bipolar derivation in the list (F8-F4) and pairing it with every other bipolar derivation according to their order on the list (F8-F4:F7-F3, F8-F4:F4-C4, F8-F4:F3-C3, etc.). The process was repeated for all other channels until the end of the list. However, since each channel is bipolar in nature, any pair with common electrode locations (such as F8-F4 and F4-C4) is neglected as this could lead to misleading high false correlation between the pair. A total of 46 channel pairs have this characteristic, and 207 bipolar pairs are therefore analysed in this paper.

In order to compare the effectiveness of cross-spectrum based on RHHT and CWT in feature extraction for the potential classification between epileptic patients and HC, we normalized each 10s epoch of EO and EC for all epileptic patients and HC. Then, the cross-spectrum values of all 207 pairs for EO and EC were calculated. Next, RHHT and CWT cross-spectra were averaged along both the time and frequency axis to obtain a singular value for each pair. Finally, 207 averaged cross-spectrum values were assessed by the Mann-Whitney U test for two groups. Fig. S1 in the Supplementary Material illustrates the p-values of each band of EC and EO data obtained through the RHHT and CWT cross-spectrum.

To quantitatively compare the performance of RHHT and CWT cross-spectrum to differentiate these two groups, we selected the top 10 smallest p-values of the 207 pairs in each frequency band of EO and EC data. Fig. 7(a) and (b) present the boxplots of EC and EO data, respectively. The red dashed line indicates the critical probability level ($p = 0.05$) that can effectively distinguish epileptic patients and HC. For both Fig. 7(a) and (b), in Theta, Alpha, and Beta bands, the distributions of the 10 smallest p-values of RHHT and CWT cross-spectrum are all higher than 0.05, which indicates invalid discrimination and will not be discussed further.

In Fig. 7(a), the distributions of the smallest 10 p-values of RHHT cross-spectrum in Delta, Gamma, and 1-50Hz bands are all lower than 0.05, while the distribution of CWT cross-spectrum in Delta and 1-50Hz bands are above the threshold. The smallest 10 p-values of CWT cross-spectrum only distributes below 0.05 in Gamma band, but the mean value of its distribution is still higher than that of RHHT cross-spectrum.

In Fig. 7(b), distributions of the smallest 10 p-values in Delta, Gamma, and 1-50Hz bands of RHHT cross-spectrum are lower than 0.05 overall, whereas distribution of CWT cross-spectrum is only lower than 0.05 in Delta and Gamma bands. Although the distribution of CWT cross-spectrum in Delta band is lower than that of RHHT cross-spectrum, the distribution of CWT cross-spectrum in Gamma band is higher than that of RHHT cross-spectrum, and the distribution of CWT cross-spectrum in 1-50Hz band spans $p = 0.05$.

In order to test the effect of epoch length on the p-values, we split the 10s epoch into different lengths and calculated the corresponding p-values. By counting the effective bipolar

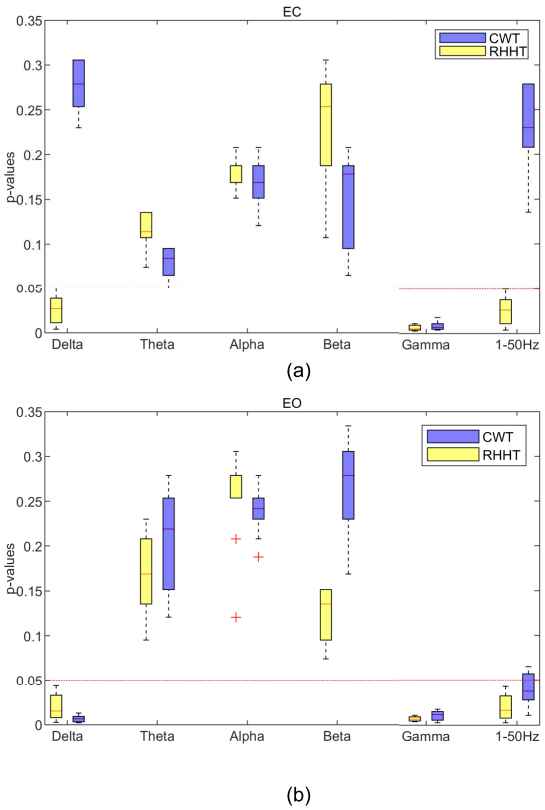

Fig. 7. The boxplots of top 10 smallest p-values of all 207 pairs for each frequency band of EC (a) and EO (b) data by RHHT and CWT cross-spectrum.

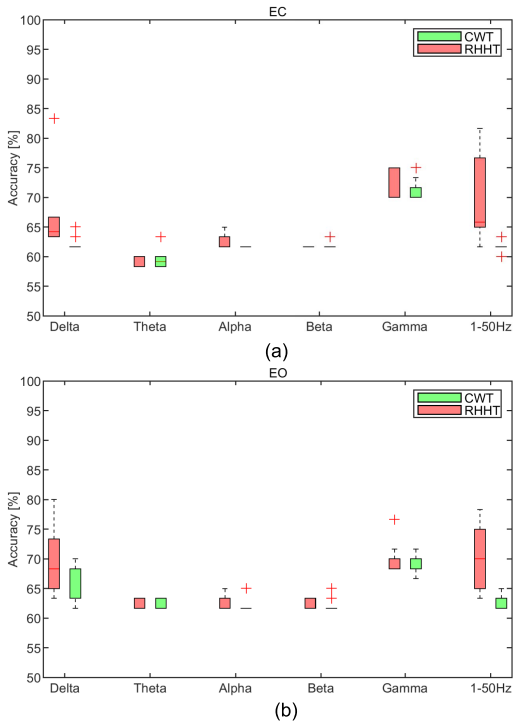

Fig. 8. The boxplots of top 10 higest classification accuracies of all 207 pairs for each frequency band of EC (a) and EO (b) data by RHHT and CWT cross-spectrum.

pairs with p-values less than 0.05, we calculated the mean numbers for each segment length. The statistical results are shown in Table S2 in the Supplementary Material. It suggests that for both RHHT and CWT cross-spectrum, the length of data samples has a negligible effect on the number of effective pairs. Similar to the results of 10s data, other data lengths (5s, 2.5s, 1.25s, and 0.625s) confirm the conclusion that RHHT cross-spectrum can reveal more distinguishable bipolar pairs than CWT in most frequency bands.

C. Classification Results Using Support Vector Machine (SVM)

We conducted a direct classification of HC and epilepsy groups using the extracted 207 cross-spectrum features from RHHT and CWT. During the initial development of the classification solution, a few popular machine learning classifiers were implemented including SVM, decision tree and k-nearest neighbors (KNN). SVM was selected as the classifier in this work because it presents slightly better performance than other methods. The classification accuracy was calculated by 10 folder cross-validation.

The boxplots of 10-highest accuracy within all bipolar pairs of EC and EO data are shown in Fig. 8(a) and (b) respectively. The classification results are in agreement with the p-values calculated by Mann-Whitney U-test shown in Fig. 7. In the three frequency bands with p-values less than 0.05 (Delta, Gamma, 1-50Hz), the classification results of SVM are better than the other three bands for both eye conditions. The average classification results of the cross-spectrum based on RHHT are higher than CWT although it has a slightly larger variation.

V. Conclusion

This paper proposes a novel data analysis framework to track the dynamic association between EEG channels in the time-frequency domain. This framework aims to characterize frequency fluctuations with a high time-frequency resolution and capture the dynamic association in the frequency domain using a new indicator, called Revised Hilbert-Huang Transformation cross-spectrum. It has been demonstrated by the two simulation examples that, compared to CWT, RHHT can estimate the frequency modulations more accurately, as well as detect the abrupt change of frequency, amplitude, and corresponding associations. This characterisation will potentially provide more insight when applied to real EEG signals which are dominated by high non-linearity and non-stationarity. Implementation of the significant test on the proposed RHHT based cross-spectrum allows identification of the significant interactions by taking into account the effects of noise interference. The application of the proposed method on EEG data from 14 epileptic patients and 10 healthy controls further demonstrates the validity of this framework and its potential application in building benchmarks for classification. In the real EEG data paradigm, we have shown with the implementation of a statistical significance approach, the estimated cross-spectrum using RHHT can better distinguish these two groups than that using CWT. However, it should be noted that a further study is required to deeply understand what additional information of RHHT contributes to the improved classification by exploring the ground truth of brain cross-sprectum.

REFERENCES

[1] M. X. Cohen, "Where does EEG come from and what does it mean?" *Trends Neurosci.*, vol. 40, no. 4, pp. 208–218, Apr. 2017.

[2] M. X. Cohen, *Analyzing Neural Time Series Data: Theory and Practice*. Cambridge, MA, USA: MIT Press, 2014.

[3] X. Navarro, F. Porée, A. Beuchée, and G. Carrault, "Denoising preterm EEG by signal decomposition and adaptive filtering: A comparative study," *Med. Eng. Phys.*, vol. 37, no. 3, pp. 315–320, Mar. 2015.

[4] G. Korats, S. Le Cam, R. Ranta, and V. Louis-Dorr, "A space-time-frequency dictionary for sparse cortical source localization," *IEEE Trans. Biomed. Eng.*, vol. 63, no. 9, pp. 1966–1973, Sep. 2016.

[5] O. Faust, U. R. Acharya, H. Adeli, and A. Adeli, "Wavelet-based EEG processing for computer-aided seizure detection and epilepsy diagnosis," *Seizure*, vol. 26, pp. 56–64, Mar. 2015.

[6] Y. Zhang, B. Liu, X. Ji, and D. Huang, "Classification of EEG signals based on autoregressive model and wavelet packet decomposition," *Neural Process. Lett.*, vol. 45, no. 2, pp. 365–378, Apr. 2017.

[7] N. E. Huang *et al.*, "The empirical mode decomposition and the Hilbert spectrum for nonlinear and non-stationary time series analysis," *Proc. Roy. Soc. London. A, Math., Phys. Eng. Sci.*, vol. 454, no. 1971, pp. 903–995, Mar. 1998.

[8] S. R. Jones, "When brain rhythms aren't 'rhythmic': Implication for their mechanisms and meaning," *Current Opinion Neurobiol.*, vol. 40, pp. 72–80, Oct. 2016.

[9] A. Mazaheri and O. Jensen, "Asymmetric amplitude modulations of brain oscillations generate slow evoked responses," *J. Neurosci.*, vol. 28, no. 31, pp. 7781–7787, Jul. 2008.

[10] M. X. Cohen, "Multivariate cross-frequency coupling via generalized eigendecomposition," *eLife*, vol. 6, Jan. 2017, Art. no. e21792.

[11] A. de Cheveigné, "Time-shift denoising source separation," *J. Neurosci. Methods*, vol. 189, no. 1, pp. 113–120, May 2010.

[12] Z. Wu and N. E. Huang, "Ensemble empirical mode decomposition: A noise-assisted data analysis method," *Adv. Adapt. Data Anal.*, vol. 1, no. 1, pp. 1–41, Jan. 2009.

[13] G. Rilling, P. Flandrin, P. Goncalves, and J. M. Lilly, "Bivariate empirical mode decomposition," *IEEE Signal Process. Lett.*, vol. 14, no. 12, pp. 936–939, Dec. 2007.

[14] N. Rehman and D. P. Mandic, "Multivariate empirical mode decomposition," *Proc. Roy. Soc. A, Math., Phys. Eng. Sci.*, vol. 466, no. 2117, pp. 1291–1302, 2010.

[15] M. E. Torres, M. A. Colominas, G. Schlotthauer, and P. Flandrin, "A complete ensemble empirical mode decomposition with adaptive noise," in *Proc. IEEE Int. Conf. Acoust., Speech Signal Process. (ICASSP)*, May 2011, pp. 4144–4147.

[16] S. Aydore, D. Pantazis, and R. M. Leahy, "A note on the phase locking value and its properties," *NeuroImage*, vol. 74, pp. 231–244, Jul. 2013.

[17] E. M. Schumacher, T. A. Stiris, and P. G. Larsson, "Effective connectivity in long-term EEG monitoring in preterm infants," *Clin. Neurophysiol.*, vol. 126, no. 12, pp. 2261–2268, Dec. 2015.

[18] M. Hamedi, S.-H. Salleh, and A. M. Noor, "Electroencephalographic motor imagery brain connectivity analysis for BCI: A review," *Neural Comput.*, vol. 28, no. 6, pp. 999–1041, Jun. 2016.

[19] B. Akbarian and A. Erfanian, "A framework for seizure detection using effective connectivity, graph theory, and multi-level modular network," *Biomed. Signal Process. Control*, vol. 59, May 2020, Art. no. 101878.

[20] K. J. Friston, "Functional and effective connectivity: A review," *Brain Connectivity*, vol. 1, no. 1, pp. 13–36, Jan. 2011.

[21] G. Marrelec, J. Daunizeau, M. Pelegrini-Issac, J. Doyon, and H. Benali, "Conditional correlation as a measure of mediated interactivity in fMRI and MEG/EEG," *IEEE Trans. Signal Process.*, vol. 53, no. 9, pp. 3503–3516, Sep. 2005.

[22] J. Chiang, Z. J. Wang, and M. J. McKeown, "A generalized multivariate autoregressive (GmAR)-based approach for EEG source connectivity analysis," *IEEE Trans. Signal Process.*, vol. 60, no. 1, pp. 453–465, Jan. 2012.

[23] R. Guevara Erra, J. L. Perez Velazquez, and M. Rosenblum, "Neural synchronization from the perspective of non-linear dynamics," *Frontiers Comput. Neurosci.*, vol. 11, p. 98, Oct. 2017, doi: 10.3389/fncom.2017.00098.

[24] P. J. Uhlhaas and W. Singer, "Neural synchrony in brain disorders: Relevance for cognitive dysfunctions and pathophysiology," *Neuron*, vol. 52, no. 1, pp. 155–168, Oct. 2006, doi: 10.1016/j.neuron.2006.09.020.

[25] E. van Diessen *et al.*, "Opportunities and methodological challenges in EEG and MEG resting state functional brain network research," *Clin. Neurophysiol.*, vol. 126, no. 8, pp. 1468–1481, Aug. 2015.

[26] C. Babiloni *et al.*, "Brain neural synchronization and functional coupling in Alzheimer's disease as revealed by resting state EEG rhythms," *Int. J. Psychophysiol.*, vol. 103, pp. 88–102, May 2016.

[27] M. Boersma, D. J. A. Smit, D. I. Boomsma, E. J. C. De Geus, H. A. de Waal, and C. J. Stam, "Growing trees in child brains: Graph theoretical analysis of electroencephalography-derived minimum spanning tree in 5- and 7-year-old children reflects brain maturation," *Brain Connectivity*, vol. 3, no. 1, pp. 50–60, 2013.

[28] N. M. Schutte, N. K. Hansell, E. J. C. de Geus, N. G. Martin, M. J. Wright, and D. J. A. Smit, "Heritability of resting state EEG functional connectivity patterns," *Twin Res. Human Genet.*, vol. 16, no. 5, pp. 962–969, Oct. 2013.

[29] F. Wendling, P. Chauvel, A. Biraben, and F. Bartolomei, "From intracerebral EEG signals to brain connectivity: Identification of epileptogenic networks in partial epilepsy," *Frontiers Syst. Neurosci.*, vol. 4, p. 154, Nov. 2010, doi: 10.3389/fnsys.2010.00154.

[30] P. van Mierlo *et al.*, "Functional brain connectivity from EEG in epilepsy: Seizure prediction and epileptogenic focus localization," *Prog. Neurobiol.*, vol. 121, pp. 19–35, Oct. 2014.

[31] F. Vecchio *et al.*, "Cortical connectivity and memory performance in cognitive decline: A study via graph theory from EEG data," *Neuroscience*, vol. 316, pp. 143–150, Mar. 2016.

[32] R. Vicente, M. Wibral, M. Lindner, and G. Pipa, "Transfer entropy—A model-free measure of effective connectivity for the neurosciences," *J. Comput. Neurosci.*, vol. 30, no. 1, pp. 45–67, 2011.

[33] V. Sakkalis, "Review of advanced techniques for the estimation of brain connectivity measured with EEG/MEG," *Comput. Biol. Med.*, vol. 41, no. 12, pp. 1110–1117, Dec. 2011.

[34] A. Mheich, M. Hassan, M. Khalil, C. Berrou, and F. Wendling, "A new algorithm for spatiotemporal analysis of brain functional connectivity," *J. Neurosci. Methods*, vol. 242, pp. 77–81, Mar. 2015.

[35] T. F. Tafreshi, M. R. Daliri, and M. Ghodousi, "Functional and effective connectivity based features of EEG signals for object recognition," *Cognit. Neurodyn.*, vol. 13, no. 6, pp. 555–566, Dec. 2019.

[36] J.-L. Chen, T. Ros, and J. H. Gruzelier, "Dynamic changes of ICA-derived EEG functional connectivity in the resting state," *Hum. Brain Mapping*, vol. 34, no. 4, pp. 852–868, Apr. 2013.

[37] F. Wendling, K. Ansari-Asl, F. Bartolomei, and L. Senhadji, "From EEG signals to brain connectivity: A model-based evaluation of interdependence measures," *J. Neurosci. Methods*, vol. 183, no. 1, pp. 9–18, Sep. 2009.

[38] P. C. Petrantonakis and L. J. Hadjileontiadis, "Adaptive emotional information retrieval from EEG signals in the time-frequency domain," *IEEE Trans. Signal Process.*, vol. 60, no. 5, pp. 2604–2616, May 2012.

[39] Y. Zhao *et al.*, "A wavelet-based correlation analysis framework to study cerebromuscular activity in essential tremor," *Complexity*, vol. 2018, pp. 1–15, Jul. 2018, doi: 10.1155/2018/7269494.

[40] A. G. Guggisberg *et al.*, "Mapping functional connectivity in patients with brain lesions," *Ann. Neurol.*, vol. 63, no. 2, pp. 193–203, 2008.

[41] T. Schreiber and A. Schmitz, "Surrogate time series," *Phys. D: Nonlinear Phenomena*, vol. 142, nos. 3–4, pp. 346–382, Aug. 2000.

[42] J. Theiler, S. Eubank, A. Longtin, B. Galdrikian, and J. Doyne Farmer, "Testing for nonlinearity in time series: The method of surrogate data," *Phys. D: Nonlinear Phenomena*, vol. 58, nos. 1–4, pp. 77–94, Sep. 1992.

[43] Y. T. Qassim, T. Cutmore, D. James, and D. Rowlands, "FPGA implementation of Morlet continuous wavelet transform for EEG analysis," in *Proc. Int. Conf. Comput. Commun. Eng. (ICCCE)*, Jul. 2012, pp. 59–64.

[44] M. X. Cohen, "A better way to define and describe Morlet wavelets for time-frequency analysis," *NeuroImage*, vol. 199, pp. 81–86, Oct. 2019.

[45] A. Mouraux and G. D. Iannetti, "Across-trial averaging of event-related EEG responses and beyond," *Magn. Reson. Imag.*, vol. 26, no. 7, pp. 1041–1054, Sep. 2008.

[46] J. Pyrzowski, M. Siemiński, A. Sarnowska, J. Jedrzejczak, and W. M. Nyka, "Interval analysis of interictal EEG: Pathology of the alpha rhythm in focal epilepsy," *Sci. Rep.*, vol. 5, no. 1, pp. 1–10, Dec. 2015.

[47] G. D. Ruxton, "The unequal variance t-test is an underused alternative to student's t-test and the Mann–Whitney *U* test," *Behav. Ecol.*, vol. 17, no. 4, pp. 688–690, 2006.

[48] P. E. McKnight and J. Najab, "Mann–Whitney U test," in *The Corsini Encyclopedia of Psychology*, doi: 10.1002/9780470479216.corpsy0524.

[49] J. Hlinka, C. Alexakis, A. Diukova, P. F. Liddle, and D. P. Auer, "Slow EEG pattern predicts reduced intrinsic functional connectivity in the default mode network: An inter-subject analysis," *NeuroImage*, vol. 53, no. 1, pp. 239–246, Oct. 2010.